sustainability

MDPI

Article

Experimentally Identifying the Influences of Key Parameters for an Organic Rankine Cycle Using R123

Yan Gao [1], Qianxi Song [1], Wen Su [2,*], Xinxing Lin [3], Zhi Sun [4], Zhisheng Huang [1] and Yaping Gao [1]

[1] Collaborative Innovation Center of Energy Conservation & Emission Reduction, Beijing University of Civil Engineering and Architecture, Beijing 100037, China
[2] School of Energy Science and Engineering, Central South University, Changsha 410083, China
[3] Institute of Science and Technology, China Three Gorges Corporation, Beijing 100038, China
[4] Department of Mechanical Engineering, University of Canterbury, Christchurch 8041, New Zealand
* Correspondence: suwenzn@csu.edu.cn; Tel.: +86-0731-88879863

Abstract: As an efficient energy conversion technology, the organic Rankine cycle (ORC) has been widely applied in medium- and low-grade heat sources. In order to explore the experimental performance of ORC and reveal the effects of operation parameters, an experimental setup was built and R123 was selected as the working fluid. In the experiments, the heat source temperature as well as the mass flow rates of the working fluid and cooling water were controlled. Under the design conditions, the net work and cycle efficiency can, respectively, reach up to 0.55 kW and 8.7%. As for the influences of key parameters, with the increase in heat source temperature from 130 °C to 160 °C, the involved heat has a small increase, while the net work increases from 0.44 kW to 0.55 kW, and the cycle efficiency greatly increases from 6.71% to 8.72% at a mass flow rate of working fluid 25 g/s. As for the mass flow rate of cooling water, it has a similar impact on the cycle performances. The difference is that the effect of the cooling water rate is relatively smaller. At the mass flow rate 25 g/s, when the cooling water rate increases from 0.68 kg/s to 0.83 kg/s, the net work varies from 0.46 kW to 0.55 kW, the cycle efficiency increases in the range 7.41~9.4%. Furthermore, except cycle efficiency, all performances are proportional to the mass flow rate of working fluid. In the test range, the difference of cycle efficiency among different mass flow rates is less than 0.7%.

Keywords: organic Rankine cycle; experimental test; thermal efficiency

Citation: Gao, Y.; Song, Q.; Su, W.; Lin, X.; Sun, Z.; Huang, Z.; Gao, Y. Experimentally Identifying the Influences of Key Parameters for an Organic Rankine Cycle Using R123. *Sustainability* **2023**, *15*, 814. https://doi.org/10.3390/su15010814

Academic Editors: Xiaoya Li and Rui Jing

Received: 9 December 2022
Revised: 28 December 2022
Accepted: 29 December 2022
Published: 2 January 2023

1. Introduction

In order to achieve the goal of carbon peaking and carbon integration, besides vigorously developing the renewable energy, a large amount of medium and low temperature heat has to be recovered [1]. As a classical thermal power generation technology, the organic Rankine cycle (ORC), has been widely employed to convert the thermal energy of medium and low temperature [2] due to the low boiling temperature of organic working fluid and the relatively high energy conversion efficiency. In the past two decades, a significant global effort has sought to address the engineering challenges of ORC so as to promote its commercialization. The application fields of ORC include biomass energy, solar energy, geothermal energy, ocean thermal energy, waste heat recovery from internal combustion engines, and gas turbine cycle [3]. Nowadays, numerous studies have been published to theoretically and experimentally investigate the ORC [4,5].

In terms of the theoretical studies on ORC, much of the attention has focused on the selection of the working fluid, cycle configuration, design and optimization, dynamics, and control [4]. As an energy transfer fluid, the used working fluid significantly influences the thermodynamic performances and operation safety of ORC. Thus, by comprehensively considering the cycle performances and environmental properties, researchers have proposed the enumerative method and molecular design to screen the optimal fluids from numerous organics. For the enumerative method, the candidate fluids are first predetermined and

then various performances are compared for these fluids so that the optimal fluid can be determined [6]. As for the molecular design, the fluids are generated by combining groups. By comparing the performances of these generated fluids, the best fluid can be found [7]. In addition to the working fluid, the system performance is also closely related to the cycle configurations. Nowadays, on the basis of a basic ORC, researchers have developed various configurations, such as the regenerative cycle, the split regenerative cycle, the cascade cycle, and the dual-pressure cycle [8,9]. These cycles generally have different performances at different application scenarios. Thus, aiming at the characteristics of the given heat sources, suitable structures can be identified by comparing performances of different cycles. In addition, for given working fluid and cycle configuration, operation parameters have to be optimized to obtain the highest net work and the lowest cost. In the literature, the optimization consists of single- and multi-objective optimizations. The widely used optimization algorithms are the genetic algorithm [10] and particle swarm algorithm [11]. Based on the above studies, system design parameters can be obtained for a given heat source. However, in practical engineering, with the change in heat source condition and ambient temperature, the system will operate dynamically under non-rated conditions. Thus, dynamic behaviors of ORC have been investigated by researchers [12,13]. Furthermore, to ensure the high efficiency and safety of system operation, the corresponding controls were also explored [14,15].

Even though fruitful results have been obtained in the theoretical studies on ORC, these are underpinned by a large number of assumptions. Thus, before performing an engineering application of ORC, experiments are still needed to test the performance of ORC. Compared with rich theoretical studies, experimental investigations of ORC are relatively smaller due to the high experimental cost. Furthermore, although various cycle configurations have been theoretically proposed, the experiments mainly focused on the basic and regenerative ORCs. For example, Feng et al. [16] established an experimental setup of 3 kW ORC with the working fluid R123. The used expansion machine was scroll expander. With the varying of working fluid mass flow rates in the range of 0.124~0.222 kg/s and heat source temperatures in the range of 383.15~413.15 K, the behaviors of components and corresponding system performance were discussed in detail. Thereafter, the research group selected R245fa as working fluid and explored the effects of the pressure drop, degree of superheating, and condenser temperature on the system's overall performance. The maximum expander shaft power and thermal efficiency are 2.64 kW and 5.92%, respectively [17]. Based on this experimental apparatus, Li et al. [18] further examined the effects of heat source temperature on the system performances. The experimental results show that, under a temperature in the range of 353.15~373.15 K, the system efficiency is in the range of 4.9~5.6%. Furthermore, an experimental performance comparison of the basic and regenerative ORC systems was also conducted by this group. The results indicate that the basic ORC system has a higher heat source temperature utilization than the regenerative ORC system [19]. With R1233zd(E) as working fluid, Li et al. [20] also constructed another experimental test facility based on a conventional recuperative ORC system. A single-screw expander was employed as the expansion device. Under the design condition, the system can output work 11 kW. In the experiments, the best thermal efficiency can reach up to 3.6% with dry expansion. In addition, Eyerer et al. [21] further compared the experimental cycle performances between R1233zd(E) and R245fa. The results show that the maximum thermal efficiency of R1233zd(E) is 6.92% higher than that of R245fa, but the output power generated by R245fa is 12.17% higher than that of R1233zd(E). For more experiments, the interest readers can refer to the studies [5,22]. In fact, there are yet hundreds of experimental platforms to test the performance of ORC from the energetic point of view. In these experiments, the commonly considered working fluids are R123, R245fa, R134a, R600a, R601a, and R1233zd(E). As for the expansion machine, scroll, screw, vane, turbomachines, and other volumetric types are employed. Among these expanders, the scroll machine has been the most popular choice and the output power is located in the range of 0.35–7.5 kW, followed by the screw expander. However, although these experiments have explored a

large number of system operating characteristics, they mainly focus on the heat source conditions, and few experimental studies have been conducted that have specifically focused on the effects of mass flow rates of working fluid and cooling water.

The above review indicates that, for the influence of key parameters on ORC performances, experimental data are still scarce in the published literature. In view of this, an experimental test facility of basic ORC was established. The used working fluid and expansion device were R123 and scroll expander. In the experiments, the system performances of ORC were first investigated under the design conditions. After that, by varying the heat source temperature as well as the mass flow rates of working fluid and cooling water, the corresponding effects on system performances were revealed.

2. Experiments

2.1. Test facility

In this work, an experimental setup was established for a basic ORC. The cycle is composed of four thermodynamic processes, namely compression, evaporation, expansion, and condensation. The corresponding components are called as pump, evaporator, turbine, and condenser, as illustrated in Figure 1.

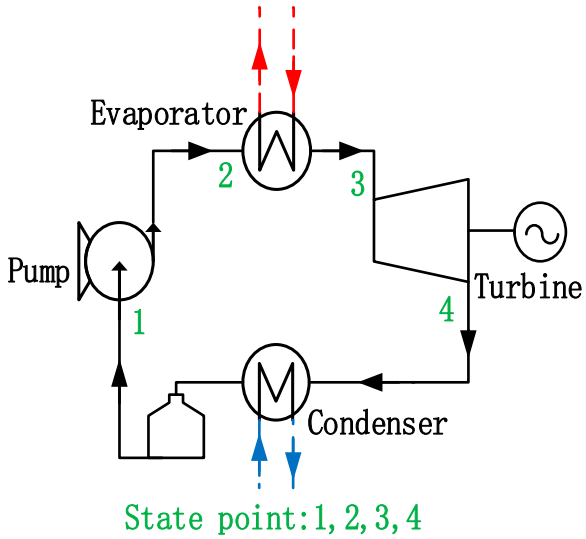

Figure 1. Schematic diagram of basic ORC.

Based on the ORC processes in Figure 1, the schematic diagram of the corresponding experimental apparatus is provided in Figure 2. It mainly consists of three parts, namely the heat source loop, working fluid loop, and cooling water loop. For the heat source loop, heat transfer oil is employed to absorb heat from the boiler and release heat to the working fluid in the evaporator. In the working fluid loop, the fluid absorbs heat from the hot oil to complete the processes of liquid preheating, evaporation, and gas superheating. Then, the high-temperature and high-pressure fluid enters the expander to generate power. After the expansion, the exhausted gas at the expander outlet flows into the condenser and is cooled into the liquid by the cooling water. After that, the liquid sequentially flows into the liquid reservoir and filter. Finally, the fluid returns to the pump and is compressed into the evaporator to complete the cycle. Furthermore, for the startup and shutdown processes, a throttle valve is employed to bypass the expander to assure the operation safety. For the cooling water loop, the water first absorbs heat in the condenser and then loses heat to the environment through the cooling tower.

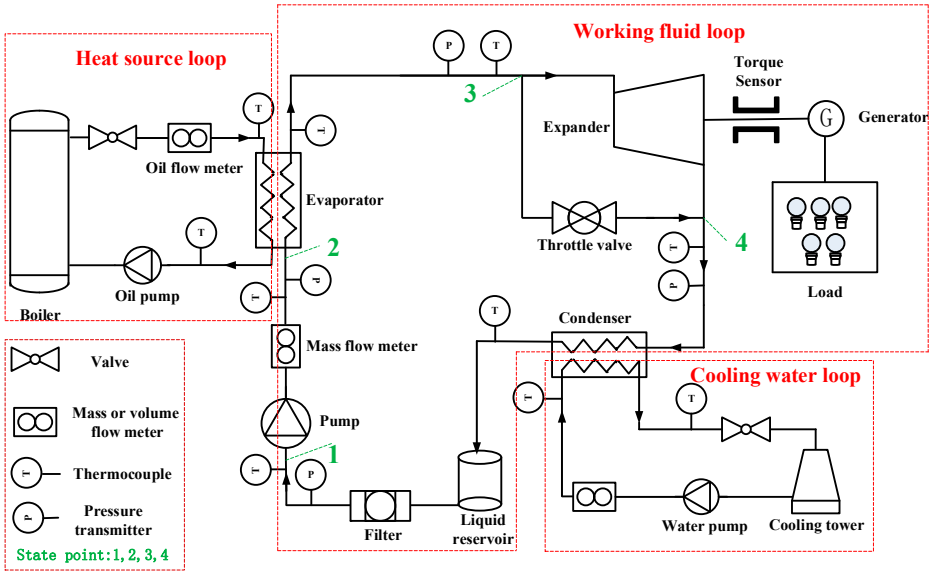

Figure 2. Schematic diagram of ORC experiment.

According to the experimental schematic diagram in Figure 2, an experimental platform was established. The real picture is given in Figure 3. As for the key components of the system, Figure 4 illustrates the real photos of the evaporator, condenser, pump, expander, cooling tower, and heat-conducting oil boiler. For the evaporator and condenser, shell and tube exchangers were used. The numbers of the shell and tube are, respectively, one and two. The corresponding heat exchange area is 5 m^2. These exchangers were manufactured and supplied by Tianjin Runren Technology Co. Ltd. (Tianjin, China) A refrigeration scroll compressor in the vehicle air conditioner was assembled as an expander, namely the inlet and outlet of compressor were reversed in the operation of expander. The designed rotation speed is 4000 r/min, and the expansion ratio is 4. For the working fluid pump, it is a diaphragm metering type manufactured by the China Southern Seper Industry. The maximum mass flow rate and working pressure are 0.25 kg/s and 1.2 MPa. The rated frequency is 50 Hz. As for the boiler, the total heating power is 20 kW, and the maximum temperature of oil can be adjusted to between 100 °C and 200 °C. Thus, the boiler has enough capacity to heat the working fluid in the experiment. For the cooling tower, the circulating volume of cooling water is 10 t/h. Since the ambient temperature of Tianjin city was 13 °C during the period of the ORC experiment, the tower could well satisfy the requirement of working fluid condensation.

Figure 3. Picture of ORC experiment.

(**a**) Shell and tube evaporator

(**b**) Shell and tube condenser

(**c**) Working fluid pump

(**d**) Scroll expander

(**e**) Cooling tower

(**f**) Heat-conducting oil boiler

Figure 4. Photos of key experimental components.

2.2. Measurements

To analyze the thermodynamic performance of the working fluid in the evaporator, condenser, pump, and expander, the temperature and pressure at the inlet and outlet of each component were, respectively, measured by the T-type thermocouples and pressure transducers, as shown in Figure 2. Furthermore, a Coriolis-type mass flow meter was employed to measure the mass flow rate of the working fluid, and a torque meter was used to determine the output work of the expander. Meanwhile, a digital power meter was used to measure the consumed power of the working fluid pump. For the heat source and cooling water loops, flow meters were installed to obtain the corresponding volume flowrates. On this basis, a data acquisition system Agilent 34980A was used to record the

current and voltage signals from the above employed instruments. The range and accuracy of each measurement instrument are provided in Table 1.

Table 1. Range and accuracy of measurement instruments.

Parameter	Instrument	Range	Accuracy
Pressure	Pressure transducer	0~1.6 MPa	±0.25% F.S.
Temperature	T-type thermocouple	−200~350 °C	±0.1 °C
Mass flow rate of working fluid	Coriolis-type mass flow meter	0~0.6 kg/s	±0.15% F.S.
Cooling water flow rate	Electromagnetic flow meter	0~8 $m^3 \cdot h^{-1}$	±0.5% F.S.
Oil flow rate	Turbine Flowmeter	0~10 $m^3 \cdot h^{-1}$	±1% F.S.
Expansion work	Torque meter	0~2 kW	±0.5% F.S.
Consumed power	Digital power meter	0~2 A	±0.5% F.S.

2.3. Test Conditions and Data Reduction

In fact, the experimental system of the ORC in Figure 3 is designed based on the working fluid R123. At present, R123 has been widely theoretically and experimentally employed in ORC [5]. Some of the thermophysical properties are provided in Table 2.

Table 2. Thermophysical properties of working fluid.

Working Fluid	Molecular Structure	Molar Mass ($g \cdot mol^{-1}$)	T_c (°C)	P_c (MPa)	T_b (°C)	Acentric Factor
R123	CF_3CHCl_2	152.93	183.68	3.66	27.82	0.282

In this work, the heat source temperature as well as the mass flow rates of the working fluid and cooling water were designed to be 160 °C, 25 g/s, and 0.83 kg/s, respectively. The inlet temperature of the cooling water was designed to be 16 °C. In order to investigate the influence of the key parameters on the system performance, the heat source temperature as well as the mass flow rates of working fluid, and cooling water were varied in the experiments. The corresponding experimental conditions are given in Tables 3 and 4. In Table 3, to reveal the effect of the heat source temperature, four temperatures, namely 130 °C, 140 °C, 150 °C, and 160 °C were considered. At each temperature, five mass flow rates of working fluid were considered, namely 13 g/s, 16 g/s, 19 g/s, 22 g/s, and 25 g/s. As for other parameters, the mass flow rate and inlet temperature of cooling water were fixed at 0.83 kg/s, 16 °C, respectively, and the ambient temperature is 13 °C. As for the effect of the cooling water flow, the mass flow rates were, respectively, set to be 0.68 kg/s, 0.73 kg/s, 0.76 kg/s, 0.8 kg/s, and 0.83 kg/s, respectively. Similarly, at each value of cooling water, the mass flow rate of working fluid varied from 13 g/s to 25 g/s at the step of 3 g/s. Furthermore, the heat source temperature and inlet temperature of cooling water were, respectively, fixed at 160 °C and 16 °C. It should be noticed that for each working condition, the experimental system was kept stably running for at least one hour, so as to obtain the corresponding cycle performances.

Table 3. Experimental conditions under the variations of heat source temperature.

Items	Values
Heat source temperature (°C)	130; 140; 150; 160
Mass flow rate of working fluid (g/s)	13; 16; 19; 22; 25
Mass flow rate of cooling water (kg/s)	0.83
Inlet temperature of cooling water (°C)	16
Ambient temperature (°C)	13

Table 4. Experimental conditions under the variations of cooling water flow.

Items	Values
Heat source temperature (°C)	160
Mass flow rate of working fluid (g/s)	13; 16; 19; 22; 25
Mass flow rate of cooling water (kg/s)	0.68; 0.73; 0.76; 0.8; 0.83
Inlet temperature of cooling water (°C)	16
Ambient temperature (°C)	13

According to the measured mass flow rate, the temperature and pressure of working fluid, the corresponding enthalpy can be obtained with the help of commercial software-REFPROP, so that various cycle performances can be calculated out at each working condition. For the evaporated heat, it is expressed by

$$\dot{Q}_{evap} = \dot{m}_{wf}(h_3 - h_2) \quad (1)$$

Similarly, the condensed heat is calculated by

$$\dot{Q}_{con} = \dot{m}_{wf}(h_4 - h_1) \quad (2)$$

As for the expander, the output work is formulated as

$$W_{exp} = \dot{m}_{wf}(h_3 - h_4) \quad (3)$$

The work consumed by pump is

$$W_{pump} = \dot{m}_{wf}(h_2 - h_1) \quad (4)$$

On this basis, the net work and cycle efficiency of ORC are defined, respectively, as

$$W_{net} = W_{exp} - W_{pump} \quad (5)$$

$$\eta = \frac{W_{net}}{\dot{Q}_{evap}} \times 100\% \quad (6)$$

2.4. Uncertainty Analysis

The experimental error comes from the measurement error and calculation error. The measurement error could be directly obtained from the provided instrument accuracy in Table 1, while the calculation error was determined by the method of Moffat [23], as expressed by Equation (7).

$$\delta U = \sqrt{\sum_{i=1}^{N} \left(\frac{\partial U}{\partial x_i}\delta x_i\right)^2} \quad (7)$$

After the calculation, the maximum uncertainties of the cycle parameters are 2.99%, 2.61%, 0.01%, 5.59%, 0.52% and 0.71%, respectively, for the evaporated heat, condensed heat, pump work, turbine work, net work and cycle efficiency.

3. Experimental Results and Discussion

In this study, more than 45 experimental runs were conducted under the given working conditions. Various experimental data were recorded in detail. On this basis, the design performances of the system were analyzed, and the influence of key operation parameters including heat source temperature as well as the mass flow rates of the working fluid and the cooling water are discussed.

3.1. Performance Analysis under the Design Conditions

Under the design conditions, the heat source temperature as well as the mass flow rates of working fluid and cooling water were controlled to be 160 °C, 25 g/s, and 0.83 kg/s,

respectively. The inlet temperature of the cooling water was fixed at 16 °C. As for the operation parameters at each state point of the ORC, Table 5 gives the corresponding temperature, pressure, and enthalpy. It can be found that the highest cycle temperature, namely the inlet temperature of expander, can reach up to 135.5 °C. The corresponding pressure is 0.76 MPa.

Table 5. Operation parameters of state points under the design conditions of ORC.

State Point	Temperature (°C)	Pressure (MPa)	Enthalpy (kJ/kg)
1	15.5	0.31	215.58
2	17.1	0.77	217.35
3	135.5	0.76	470.89
4	99.5	0.35	447.03

According to the operation parameters in Table 5, various performances of the ORC are obtained as listed in Table 6. Table 6 shows that the exchanged heats in the evaporator and condenser are, respectively, 6.3 kW and 5.75 kW. For the turbine and pump, the involved works are 0.59 kW and 0.04 kW, respectively. Thus, the net work and cycle efficiency are, respectively, at 55 kW and 8.7%.

Table 6. Performance of the ORC under the design conditions.

Components	Value
Evaporator	6.3 kW
Turbine	0.59 kW
Condenser	5.75 kW
Pump	0.04 kW
Net work	0.55 kW
Cycle efficiency	8.7%

3.2. Effects of Heat Source Temperature and Working Fluid Mass Flow Rate

At five different mass flow rates of R123, Figure 5 gives the variations of evaporated heat with the heat source temperature. It can be observed that at a certain mass flow rate, as the heat source temperature increases, the evaporated heat increases slightly overall. It can be explained by the fact that, at a higher heat source temperature, although the outlet temperature of the evaporator increases, the evaporation pressure also increases, thus resulting in a slight reduction in the enthalpy difference under the unit temperature rise. Furthermore, at a fixed heat source temperature, the more the mass flow rate, the higher the evaporated heat. When the heat source temperature is 160 °C, the heat increases from 3.44 kW at 13 g/s to 6.30 kW at 25 g/s. Thus, it can be concluded that the evaporated heat is proportional to the mass flow rate of working fluid in the same temperature experimental conditions.

Figure 6 shows the variations of condensed heat at different mass flow rates of R123. Similarly, at a certain mass flow rate of working fluid, with the increase in heat source temperature, the condensed heat experiences a small increase. This is because the outlet temperature of the expander has an increase at a higher heat source temperature. Furthermore, when the heat source temperature is fixed, the condensed heat increases with the increase in mass flow rate. At the temperature 130 °C, when the mass flow rate varies from 13 g/s to 25 g/s, the condensed heat increases from 2.96 kW to 5.53 kW. At the temperature of 160 °C, the condensed heat varies in the range of 3.11~5.75 kW.

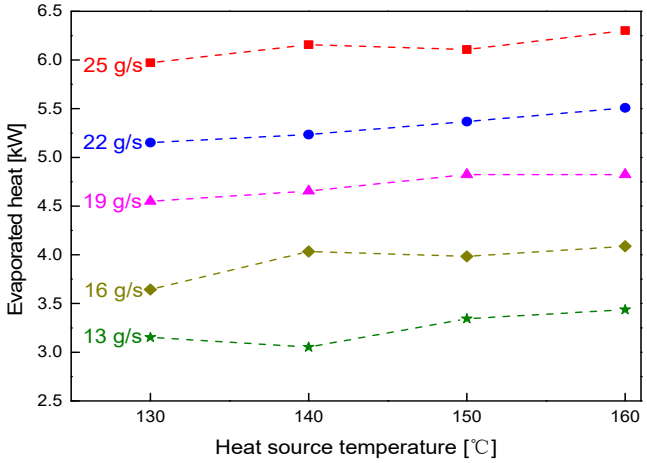

Figure 5. Effect of heat source temperature on the evaporated heat at different mass flow rates of R123.

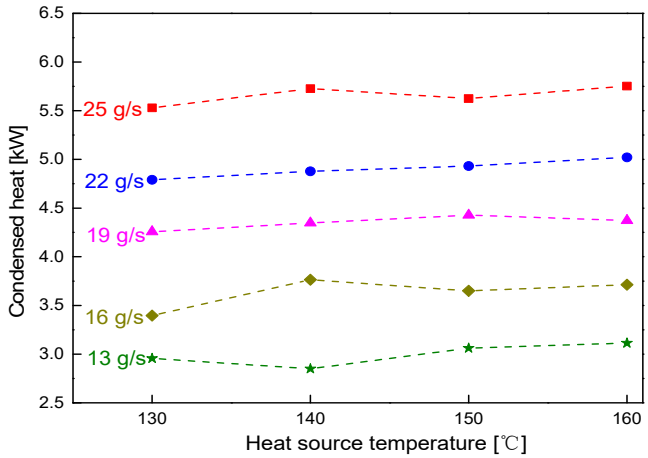

Figure 6. Effect of heat source temperature on the condensed heat at different mass flow rates of R123.

As for the net work and cycle efficiency, the corresponding variations are, respectively, given in Figures 7 and 8. Figure 7 illustrates that with the increase in heat source temperature and mass flow rate, the net work has an obvious increase. When the temperature is fixed at 130 °C, the net work varies from 0.19 kW to 0.42 kW in the considered range of 13~25 g/s. Similarly, at the temperature of 160 °C, the net work increases from 0.32 kW to 0.55 kW. Furthermore, at the mass flow rate of 25 g/s, the net work increases from 0.44 kW to 0.55 kW in the temperature range of 130~160 °C. As for the cycle efficiency in Figure 8, under the mass flow rate 25 g/s, when the temperature increases from 130 °C to 160 °C, the efficiency greatly increases from 6.71% to 8.72%. Similarly, for other mass flow rates, as the temperature increases, a great increase in cycle efficiency can be observed, especially at a higher temperature. However, for the effect of the mass flow rate, there is no obvious rule for the variation in cycle efficiency. When the heat source temperature is fixed, the difference in efficiency is less than 0.6% at different mass flow rates.

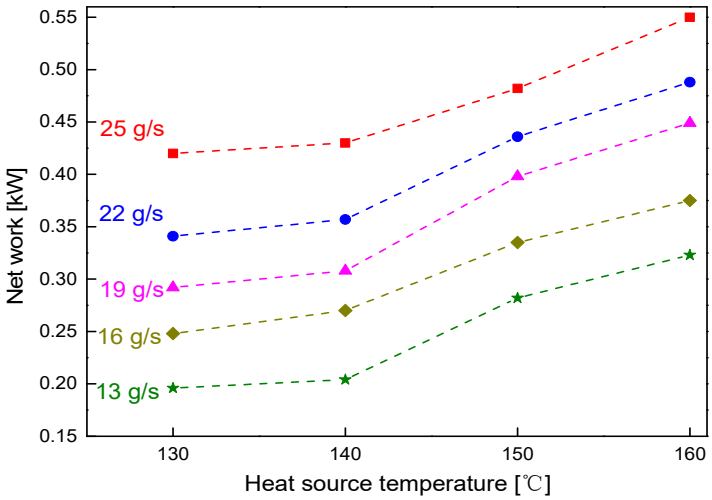

Figure 7. Effect of heat source temperature on the net work at different mass flow rates of R123.

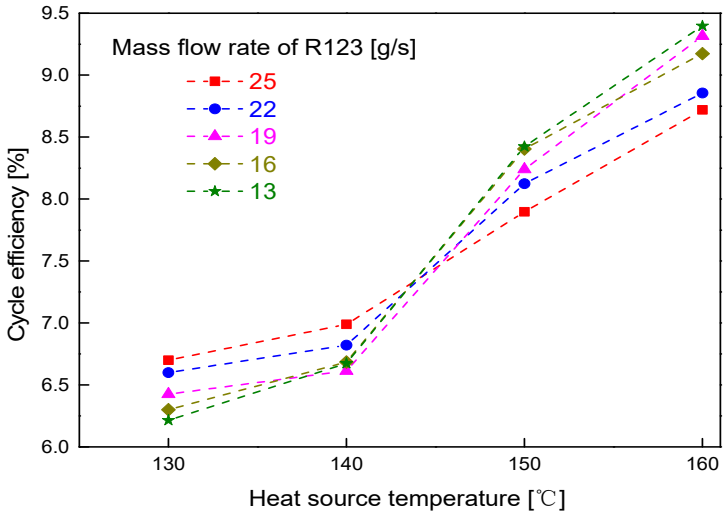

Figure 8. Effect of heat source temperature on the cycle efficiency at different mass flow rates of R123.

3.3. Effects of Cooling Water Mass Flow Rate

Besides discussing the heat source temperature and mass flow rate of the working fluid, the effect of cooling water mass flow rate was also explored. The experimental results are provided in Figures 9–12. Figure 9 gives the variations of evaporated heat with the mass flow rate of cooling water. It can be found that, when the mass flow rate of working fluid is fixed, a little variation in evaporated heat exists in the considered range of the cooling water mass flow rate. For instance, at the mass flow rate of working fluid 25 g/s, as the cooling water rate increases from 0.68 kg/s to 0.83 kg/s, the heat varies in the range of 6.18~6.3 kW. Furthermore, being similar to Figure 5, the higher the mass flow rate of working fluid, the more the heat evaporates.

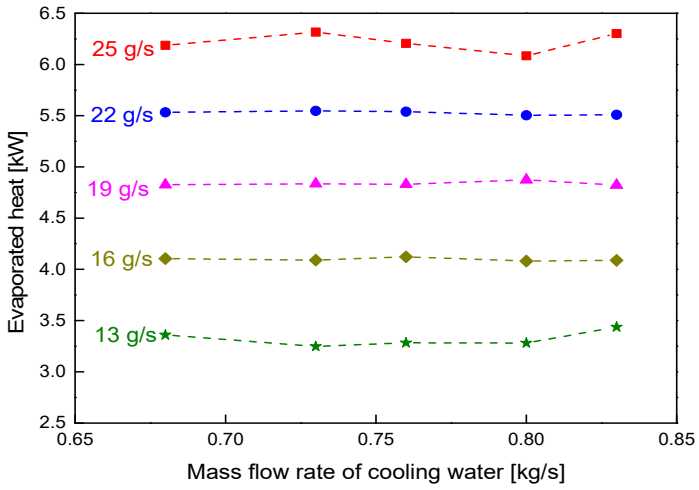

Figure 9. Effect of the cooling water mass flow rate on the evaporated heat.

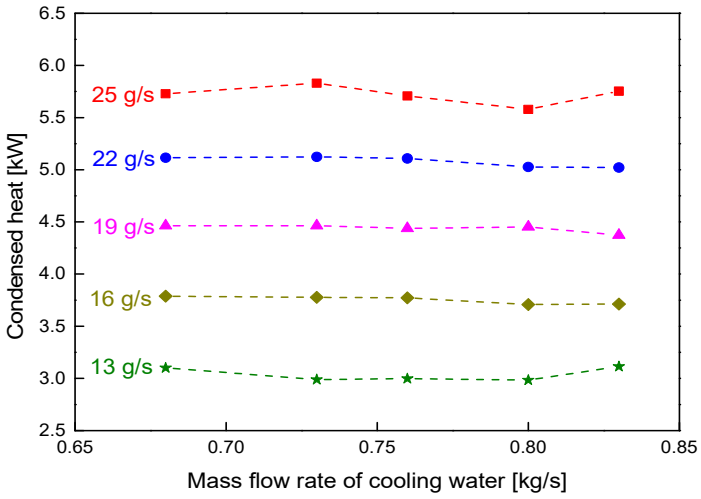

Figure 10. Effect of cooling water mass flow rate on the condensed heat.

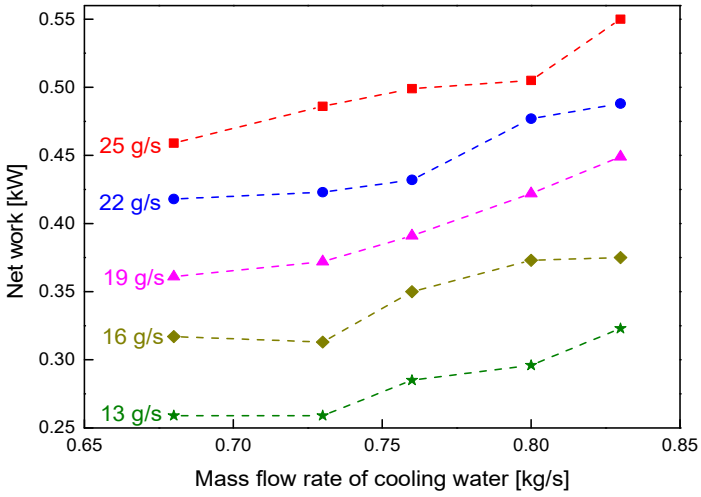

Figure 11. Effect of cooling the water mass flow rate on the net work.

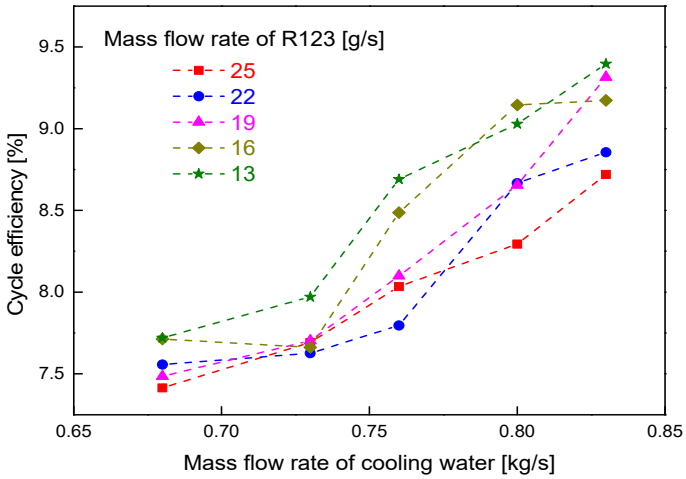

Figure 12. Effect of cooling water mass flow rate on the cycle efficiency.

For the variation in the condensed heat, Figure 10 provides the curves at different mass flow rates of the working fluids. It can be observed that these curves are similar to those of the evaporated heat. At a certain mass flow rate of the working fluid, the condensed heat varies little with the cooling water rate. For example, when the mass flow rate of working fluid is 13 g/s, the condensed heat varies in the range of 2.99~3.11 kW under the considered experimental conditions. Thus, it can be concluded that the cooling water rate almost has no obvious effect on the condensed heat.

As for the variation in the net work in Figure 11, it can be observed that with the increase in the cooling water rate, the net work experiences an increase. However, compared with the variations in Figure 7, the increase in the net work in Figure 11 is relatively smaller. At the mass flow rate of working fluid 25 g/s, when the cooling water rate increases from 0.68 kg/s to 0.83 kg/s, the net work varies from 0.46 kW to 0.55 kW. Similarly, the higher the mass flow rate of working fluid, the higher the net work is. Furthermore, for the cycle efficiency in Figure 12, it can be found that, with the increase in the cooling water rate, the efficiency increases in the range of 7.41~9.4%. For different mass flow rates of working fluid, the efficiency difference is less than 0.7% at a fixed cooling water rate.

From the above figures, the influence of key parameters has been revealed. With the increase in heat source temperature, the involved heat has a small increase, while the net work and cycle efficiency have greater improvements. The mass flow rate of the cooling water has a similar impact on the cycle performances. The difference is that the effect of the cooling water rate is smaller. Furthermore, except for cycle efficiency, all the performances are proportional to the working fluid's mass flow rate. In the test range, the working fluid's mass flow rate almost has no effect on the cycle efficiency. Despite the above results, the existing experiment only addresses the basic ORC. Meanwhile, due to the restrictions of the experimental setup, more variation ranges in heat source temperature as well as mass flow rates of the working fluid and cooling water cannot be achieved. These limitations have to be solved in future work.

4. Conclusions

By establishing the experimental setup of the organic Rankine cycle (ORC), this paper experimentally investigated the cycle performances of R123. Under the experimental conditions, the effects of the heat source temperature as well as the mass flow rates of working fluid and cooling water on the ORC performances were clarified. The relevant conclusions can be drawn as follows:

(1) Under the design conditions, the heat source temperature as well as the mass flow rates of working fluid and cooling water are 160 °C, 25 g/s, and 0.83 kg/s, respectively. The experimental system of the ORC can output a net work of 0.55 kW and reach a cycle efficiency of up to 8.7%.

(2) For the effects of the operation parameters, as the heat source temperature increases from 130 °C to 160 °C, the evaporated heat and condensed heat show small increases, while the net work and cycle efficiency increased significantly. For the cooling water rate, it has no obvious effects on the involved heat. However, the larger the mass flow rate of the cooling water, the higher the net work and cycle efficiency. Furthermore, except for the cycle efficiency, all the performances are proportional to the mass flow rate of working fluid. Under various conditions, the maximum net work is 0.55 kW and the highest efficiency is 9.40%.

Due to the limitations of the experimental setup, this work only preliminary explores the performances of basic ORC with the working fluid R123. Thus, in work to be undertaken in the near future, an internal heat exchanger will be added to the experimental apparatus, and more experimental studies will be conducted to further understand the operation characteristics of this system. Besides R123, commonly used working fluids such as R245fa, R1234yf, and R600 will be considered. Furthermore, according to the experimental data under various conditions, the non-design performance model of ORC will be developed. Meanwhile, a dynamic model is planned to be built for ORC. The simulation results will be checked by the existing experimental system and a simulation library is expected to be developed.

Author Contributions: Conceptualization, Y.G. (Yan Gao) and X.L.; methodology, W.S. and Z.H.; experiment, Q.S. and Z.S.; data curation, Y.G. (Yaping Gao); writing-original draft preparation, Y.G. (Yan Gao); writing-review and editing, W.S. All authors have read and agreed to the published version of the manuscript.

Funding: This research was funded by the Scientific Research Key Project of Beijing Educational Committee, grant number KZ202110016022, and the National Nature Science Foundation of China, grant number 52106037.

Informed Consent Statement: Informed consent was obtained from all subjects involved in the study.

Data Availability Statement: Data are available upon request.

Conflicts of Interest: The authors declared that they have no known competing financial interest or personal relationships that could have appeared to influence the work reported in this paper.

Nomenclature

Symbols

h	Enthalpy	kJ/kg
$\dot{m}$	Mass flow rate	kg/s
ORC	Organic Rankine cycle	
P	Pressure	MPa
$\dot{Q}$	Heat flow	kW
T	Temperature	K
W	Work	kW

Greeks

η	Efficiency

Subscripts

1, . . . 4	Thermodynamic state points (Figure 1)
b	Boiling temperature
c	Critical point
con	Condensation
exp	Expander
net	Net output
pump	Pump
wf	Working fluid

References

1. Lin, X.; Zuo, L.; Yin, L.; Su, W.; Ou, S. An idea to efficiently recover the waste heat of Data Centers by constructing an integrated system with carbon dioxide heat pump, mechanical subcooling cycle and lithium bromide-water absorption refrigeration cycle. *Energy Convers. Manag.* **2022**, *256*, 115398. [CrossRef]
2. Su, W.; Hwang, Y.; Deng, S.; Zhao, L.; Zhao, D. Thermodynamic performance comparison of Organic Rankine Cycle between zeotropic mixtures and pure fluids under open heat source. *Energy Convers. Manag.* **2018**, *165*, 720–737. [CrossRef]
3. Rahbar, K.; Mahmoud, S.; Al-Dadah, R.K.; Moazami, N.; Mirhadizadeh, S.A. Review of organic Rankine cycle for small-scale applications. *Energy Convers. Manag.* **2017**, *134*, 135–155. [CrossRef]
4. Imran, M.; Haglind, F.; Asim, M.; Zeb, A.J. Recent research trends in organic Rankine cycle technology: A bibliometric approach. *Renew. Sustain. Energy Rev.* **2018**, *81*, 552–562. [CrossRef]
5. Park, B.S.; Usman, M.; Imran, M.; Pesyridis, A. Review of Organic Rankine Cycle experimental data trends. *Energy Convers. Manag.* **2018**, *173*, 679–691. [CrossRef]
6. Zinsalo, J.M.; Lamarche, L.; Raymond, J. Performance analysis and working fluid selection of an Organic Rankine Cycle Power Plant coupled to an Enhanced Geothermal System. *Energy* **2022**, *245*, 123259. [CrossRef]
7. Su, W.; Zhao, L.; Deng, S. Simultaneous working fluids design and cycle optimization for Organic Rankine cycle using group contribution model. *Appl. Energy* **2017**, *202*, 618–627. [CrossRef]
8. Liu, P.; Shu, G.; Tian, H. How to approach optimal practical Organic Rankine cycle (OP-ORC) by configuration modification for diesel engine waste heat recovery. *Energy* **2019**, *174*, 543–552. [CrossRef]
9. Lecompte, S.; Huisseune, H.; van den Broek, M.; Vanslambrouck, B.; De Paepe, M. Review of organic Rankine cycle (ORC) architectures for waste heat recovery. *Renew. Sustain. Energy Rev.* **2015**, *47*, 448–461. [CrossRef]
10. Lin, X.; Chen, C.; Yu, A.; Yin, L.; Su, W. Performance Comparison of Advanced Transcritical Power Cycles with High-Temperature Working Fluids for the Engine Waste Heat Recovery. *Energies* **2021**, *14*, 5886. [CrossRef]
11. Lei, Y.; Ye, S.; Xu, Y.; Kong, C.; Xu, C.; Chen, Y.; Huang, W.; Xiao, H. Multi-objective optimization and algorithm improvement on thermal coupling of SOFC-GT-ORC integrated system. *Comput. Chem. Eng.* **2022**, *164*, 107903. [CrossRef]
12. Lin, S.; Zhao, L.; Deng, S.; Ni, J.; Zhang, Y.; Ma, M. Dynamic performance investigation for two types of ORC system driven by waste heat of automotive internal combustion engine. *Energy* **2019**, *169*, 958–971. [CrossRef]
13. Ping, X.; Yang, F.; Zhang, H.; Xing, C.; Zhang, W.; Wang, Y.; Yao, B. Dynamic response assessment and multi-objective optimization of organic Rankine cycle (ORC) under vehicle driving cycle conditions. *Energy* **2023**, *263*, 125551. [CrossRef]
14. Zhao, R.; Zhang, H.; Song, S.; Tian, Y.; Yang, Y.; Liu, Y. Integrated simulation and control strategy of the diesel engine–organic Rankine cycle (ORC) combined system. *Energy Convers. Manag.* **2018**, *156*, 639–654. [CrossRef]
15. Liu, C.; Gao, T. Off-design performance analysis of basic ORC, ORC using zeotropic mixtures and composition-adjustable ORC under optimal control strategy. *Energy* **2019**, *171*, 95–108. [CrossRef]
16. Feng, Y.Q.; Hung, T.C.; Wu, S.L.; Lin, C.H.; Li, B.X.; Huang, K.C.; Qin, J. Operation characteristic of a R123-based organic Rankine cycle depending on working fluid mass flow rates and heat source temperatures. *Energy Convers. Manag.* **2017**, *131*, 55–68. [CrossRef]
17. Yang, S.C.; Hung, T.C.; Feng, Y.Q.; Wu, C.J.; Wong, K.W.; Huang, K.C. Experimental investigation on a 3 kW organic Rankine cycle for low-grade waste heat under different operation parameters. *Appl. Therm. Eng.* **2017**, *113*, 756–764. [CrossRef]
18. Li, Y.M.; Hung, T.C.; Wu, C.J.; Su, T.Y.; Xi, H.; Wang, C.C.; Lund, H.; Kaiser, M.J. Experimental investigation of 3-kW organic Rankine cycle (ORC) system subject to heat source conditions: A new appraisal for assessment. *Energy* **2021**, *217*, 119342. [CrossRef]
19. Feng, Y.Q.; Wang, X.; Niaz, H.; Hung, T.C.; He, Z.X.; Zeb, A.J.; Xi, H. Experimental comparison of the performance of basic and regenerative organic Rankine cycles. *Energy Convers. Manag.* **2020**, *223*, 113459. [CrossRef]
20. Li, X.; Lecompte, S.; Nieuwenhuyse, J.V.; Couvreur, K.; Markides, C.N. Experimental investigation of an organic Rankine cycle with liquid-flooded expansion and R1233zd(E) as working fluid. *Energy Convers. Manag.* **2021**, *234*, 113894. [CrossRef]
21. Eyerer, S.; Wieland, C.; Vandersickel, A.; Spliethoff, H. Experimental study of an ORC (Organic Rankine Cycle) and analysis of R1233zd-E as a drop-in replacement for R245fa for low temperature heat utilization. *Energy* **2016**, *103*, 660–671. [CrossRef]
22. Tian, H.; Liu, P.; Shu, G. Challenges and opportunities of Rankine cycle for waste heat recovery from internal combustion engine. *Prog. Energy Combust. Sci.* **2021**, *84*, 100906. [CrossRef]
23. Moffat, R.J. Describing the uncertainties in experimental results. *Exp. Therm. Fluid Sci.* **1988**, *1*, 3–17. [CrossRef]